Monthly Notices of the ROYAL ASTRONOMICAL SOCIETY

MNRAS **524,** 3741–3748 (2023) https://doi.org/10.1093/mnras/stad2106
Advance Access publication 2023 July 13

Formation of H_2 on polycyclic aromatic hydrocarbons under conditions of the ISM: an ab initio molecular dynamics study

Nicolás F. Barrera,[1] Patricio Fuentealba,[1,2] Francisco Muñoz,[1,2]★ Tatiana Gómez[3] and Carlos Cárdenas[1,2]★

[1]*Departamento de Física, Facultad de Ciencias, Universidad de Chile, Av. Las Palmeras 3425, Ñuñoa, Santiago, Chile*
[2]*Centro para el Desarrollo de la Nanociencia y la Nanotecnología (CEDENNA), Av. Ecuador 3493, Santiago 9170124, Chile*
[3]*Theoretical and Computational Chemistry Center, Institute of Applied Chemical Sciences, Faculty of Engineering, Universidad Autónoma de Chile, Santiago, Chile*

Accepted 2023 July 9. Received 2023 July 6; in original form 2023 May 23

ABSTRACT

Understanding how the H_2 molecule is formed under the chemical conditions of the interstellar medium (ISM) is critical to the whole chemistry of it. Formation of H_2 in the ISM requires a third body acting as a reservoir of energy. Polycyclic aromatic hydrocarbons (PAHs) are excellent candidates to play that role. In this work, we simulated the collisions of hydrogen atoms with coronene to form H_2 via the Eley–Rideal mechanism. To do so, we used Born–Oppenheimer (*ab initio*) molecular dynamics simulations. Our results show that adsorption of H atoms and subsequent release of H_2 readily happen on coronene for H atoms with kinetic energy as large as 1 eV. Special attention is paid to dissipation and partition of the energy released in the reactions. The capacity of coronene to dissipate collision and reaction energies varies with the reaction site. Inner sites dissipate energy easier and faster than edge sites, thus evidencing an interplay between the potential energy surface around the reaction centre and its ability to cool the projectile. As for the recombination of H atoms and the subsequent formation of H_2, it is observed that ~ 15 per cent of the energy is dissipated by the coronene molecule as vibrational energy and the remaining energy is carried by H_2. The H_2 molecules desorb from coronene with an excited vibrational state ($\upsilon \geq 3$), a large amount of translational kinetic energy ($\geq$0.4 eV), and with a small activation of the rotational degree of freedom.

Key words: astrochemistry – molecular processes – ISM: molecules.

1 INTRODUCTION

Molecular hydrogen is the most abundant molecule in the Universe (Vidali 2013; Wakelam et al. 2017). Hence, H_2 plays a key role in the physical and chemical properties of the interstellar medium (ISM) as it acts as a cooling/heating agent, triggers the collapse of molecular clouds which lead to star formation, and it is a precursor in networks of chemical reactions in interstellar dust and molecular clouds (Le Page, Snow & Bierbaum 2009; Barrales-Martínez, Cortés-Arriagada & Gutiérrez-Oliva 2018). For example, H_2 facilitates the formation of molecules and ions such as CO, H_2O, HCN, HCO^+, and H_3^+ (Boschman et al. 2015). The mechanisms by which H_2 could be formed in the conditions of the ISM are not completely understood. What is clear is that abundance of H_2 in the ISM cannot be explained as the direct association of two H atoms in gas phase (Mennella et al. 2012; Vidali 2013; Wakelam et al. 2017). H_2 formation is a very exothermic process and the ∼4.5 eV released in the reaction cannot be effectively dissipated by the particle density of the ISM. The consensus is that H_2 formation takes place mainly on dust grains, which act as reservoir that can absorb part of the energy released in the association reaction (van de Hulst 1948; Gould & Salpeter 1963; Lemaire et al. 2010; Pantaleone et al. 2021). There is evidence that, under conditions relevant to the ISM, H_2 forms on surfaces of silicates (Pirronello et al. 1997; Lemaire et al. 2010), amorphous water (Roser et al. 2003), graphite, carbonaceous material (Latimer, Islam & Price 2008), and polycyclic aromatic hydrocarbons (PAHs; Bauschlicher 1998; Roser et al. 2003; Thrower et al. 2012).

Interstellar dust grain surfaces have several mechanisms for H_2 formation. Two of primary importance are the Langmuir–Hinshelwood (LH) and the Eley–Rideal (ER) mechanisms (Bauschlicher 1998; Mennella et al. 2012). The LH mechanism involves atoms being absorbed on the surface from the gas phase, diffusing and then reacting. Depending on how the energy released in the reaction is accommodated by the host grain, H_2 molecules might or might not leave the surface. In contrast, the ER mechanism involves chemisorption of an H atom on the surface and a second H atom impacting the cross-section of the first to abstract it, forming H_2 by recombination. The nascent H_2 molecule is likely to leave the surface with much of the energy released in the reaction (Wakelam et al. 2017). Both mechanisms require hydrogen atoms to absorb on the surface of the dust grain. As the grain temperature increases, physisorbed H atoms start to evaporate, and only chemisorbed H atoms remain on the dust grain surface. Therefore, the LH mechanism becomes less efficient, and H_2 formation relies on the ER mechanism. Physisorbed H atoms desorb at grain temperatures between 10 and 20 K (Cazaux & Spaans 2009).

Although the formation of molecular hydrogen via dust grains in the ISM is widely accepted, there are still gaps in our knowledge, particularly in high kinetic energy/temperature conditions and on

★ E-mail: pfuentea@hotmail.es (PF); cardena@uchile.cl (CC)

© 2023 The Author(s)
Published by Oxford University Press on behalf of Royal Astronomical Society

Downloaded from https://academic.oup.com/mnras/article/524/3/3741/7224009 by guest on 27 March 2024

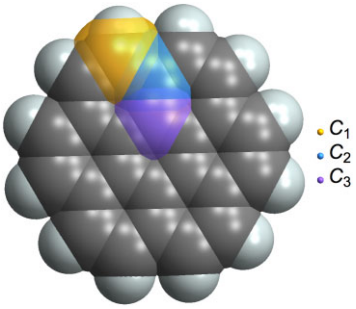

Figure 1. Labels of the different adsorption sites on coronene. The colours show the equivalent carbons in a particular ring.

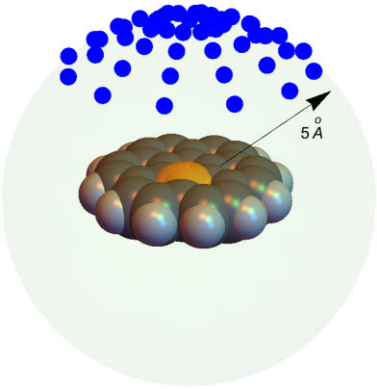

Figure 2. Initial position of H atoms used for the molecular dynamics of the collision of H · and coronene. Each blue point on the surface represents an initial position of the H · projectile. The 49 points (blue) are distributed over the surface of the spherical cap of radius 5 Å and centred in the target atom (orange), which could be a carbon (for chemisorption) or adsorbed H (for H_2 abstraction).

surfaces different than ice water (Vidali 2013; Wakelam et al. 2017). Some researchers proposed that PAHs may play a key role in H_2 formation. PAHs are components of interstellar dust grains found in various environments throughout the ISM (Tielens 2008; Burke & Brown 2010). They are estimated to account for 2–30 per cent of the carbon in the ISM (Tielens 2008) and amount up to half of the total dust grain surface area available for chemical reactions (Weingartner & Draine 2001). Recently, researchers detected PAH molecules in the TMC-1 molecular cloud, including 1- and 2-cyanonaphthalene (McCarthy & McGuire 2021; McGuire et al. 2021) and indene (Cernicharo et al. 2021). Previous experimental and theoretical studies have established the potential of PAHs as catalysts for H_2 formation (Thrower et al. 2012; Boschman et al. 2015; Foley et al. 2018; Barrales-Martínez & Gutiérrez-Oliva 2019). For instance, a prototypical PAH molecule, pyrene, has a barrierless reaction channel for H_2 recombination in the singlet state (ground state), but a barrier in the triplet state (Barrales-Martínez et al. 2018).

We examine the dynamics of chemisorption of H atoms and the formation of H_2 on coronene, a prototype PAH, under conditions relevant to the ISM and adopting the ER reaction mechanism. Since these reactions release significant amounts of energy (Cortés-Arriagada et al. 2014; Wakelam et al. 2017) ($\Delta E \leq -0.6$ eV), we are interested in understanding coronene's ability to absorb the energy generated by both reactions under different impact parameters. We also aim to gain insight into the distribution of kinetic energy of the nascent H_2 molecule, which other authors have referred to as the fate of the energy released in the formation of H_2 (Lemaire et al. 2010; Pantaleone et al. 2021). We employed Born–Oppenheimer molecular dynamics (BOMD) of the impact of H · projectiles on coronene ($C_{24}H_{12}$). Previously, BOMD has been used to study the dissipation of the energy released in H_2 formation (Pantaleone et al. 2021), and also coronene has been used in the past as a model of H_2 formation on cations of PAH (Foley et al. 2018). The remainder of this article is organized as follows. In Section 2, we describe the computational and chemical model. The results of our simulations and their implications are presented and discussed in Section 3. We conclude in Section 4.

2 COMPUTATIONAL DETAILS

We used a coronene molecule as a prototype of PAH in collision with H atoms. We assume that the coronene molecule is in the equilibrium geometry of its electronic singlet ground state (see Fig. 1). We used BOMD in the microcanonical ensemble, i.e. at constant energy and number of atoms. This ensemble fits best the conditions of the ISM where the low concentration of particles hinders the dissipation of thermal energy on time-scales of the collision (<500 fs). Similar set-ups have been used by Inostroza et al. (2019) and others (Inostroza-Pino et al. 2020; Chen et al. 2021; Inostroza-Pino et al. 2021; Pantaleone et al. 2021) to simulate molecular collisions in the ISM.

Electronic states, energies, and forces on atoms were calculated using density-functional tight-binding method (SCC-DFTB or also called DFTB2), a parametrized quantum chemical method derived from density functional theory (DFT) based on a second-order expansion of the DFT total energy around a reference density (Foulkes & Haydock 1989; Koskinen & Mäkinen 2009; Elstner & Seifert 2014). In particular, for the first step of ER mechanism (chemisorption), we used the spin-polarized DFTB2 with MIO Slater–Koster parameter set (Elstner et al. 1998; Köhler, Seifert & Frauenheim 2005). All these calculations were carried out using DFTB+ package (Hourahine et al. 2020). For the second step (abstraction), we used the uDFTB2 with MIO set of parameters augmented with MIOmod parameters for the H–H potential (Elstner et al. 1998). We chose MIOmod H–H parameters over the MIO because the former allows a better description of the atomization energy, bond length, and vibrational frequency of the H_2 molecule. All these calculations were done with GAUSSIAN 09 (Frisch et al. 2009). We tested the suitability of the tight-binding parametrization by comparing the potential energy of randomly selected trajectories with DFT calculation employing PBE functional (Perdew, Burke & Ernzerhof 1996) and the same basis set, 6–31G(d), as the DFTB parametrizations (see Section 2 in Supporting Information). Finally, we used the Verlet-velocity algorithm to integrate the equations of motion. A assessment of the conservation of energy indicates that a time-step of 0.2 fs guarantees conservation within a 50 meV interval during the whole simulation.

As coronene belongs to D_{6h} point group, it has three non-equivalent carbons, which we labelled C_1, C_2, and C_3 in Fig. 1. For each site, 49 projectiles were launched from an spherical cap of radius 5 Å centred in the target carbon (see Fig. 2). This distance prevents energy transfer (interactions) between the surface and the projectile at the beginning of the molecular dynamics. The cap was discretized with the polar angle ranging from 0° to 40° with a step of 10°, while the azimuthal angle ranges from 0° to 360° with 30° step. Three values of initial kinetic energy of the H projectile were used for each carbon site: (i) a value slightly higher than the reaction barrier, (ii) 0.50, and (iii) 1.00 eV.

Downloaded from https://academic.oup.com/mnras/article/524/3/3741/7224009 by guest on 27 March 2024

Table 1. Activation energy $\Delta E^{\ddagger}$, reaction energy ΔE°, and impact energies K_i of hydrogen projectiles for each site. All values in eV.

Site $C_i (i = 1 - 3)$	$\Delta E^{\ddagger}$	ΔE°	Energy of projectiles K (eV)
1	0.060	−1.45	0.06, 0.5, 1.0
2	0.220	−0.74	0.26, 0.5, 1.0
3	0.196	−0.63	0.22, 0.5, 1.0

3 RESULTS AND DISCUSSION

3.1 Chemisorption of a single hydrogen atom

In the ER mechanism, the initial step involves the chemisorption of the incoming hydrogen atom on any of the three available sites, which have different properties. The reactions are exothermic and have reaction barriers (see Table 1). The smallest selected kinetic energy of the projectiles is slightly higher than the reaction barrier to allow trajectories where the reaction occurs. The regime of medium (0.5 eV) and large (1.0 eV) kinetic energy is also explored. We analysed the energetics of the dynamics in two steps. First, we examined how likely it is for H · projectiles to stick to the molecule. Second, we investigated how much energy the reactive site retains, and how quickly this energy dissipates to the rest of the molecule.

The hydrogen atom hitting the coronene with kinetic energy higher than the minimum reaction barrier does not always result in H chemisorption. This depends on the orientation of the projectile and its kinetic energy. When the kinetic energy is only marginally greater than the barrier, collisions might not be reactive because the impact channel does not coincide with the minimum energy path, which is perpendicular collision (polar angle = 0°). This is clear from Fig. 3 where the sticking coefficient (the fraction of incoming H that adsorb on coronene) is plotted as a function of the projectile kinetic energy and polar angle. At the lowest projectile kinetic energy, the chance of H to adsorb greatly depends on the polar angle. This dependence, however, does not follow the dependence expected in thermal equilibrium (i.e. $\propto \cos^2(\theta)$). The general trend is that sticking probability decreases as the projectile deviates from normal impact and it is completely suppressed for slant impacts on the innermost carbon (C_3). As the projectile kinetic energy increases to 0.5 and 1.0 eV, the sticking probability for non-normal impacts markedly increases. For instance, for a projectile with 1 eV of kinetic energy at least 70 per cent of impacts at low polar angle (40°) result in chemical adsorption of the H on the carbon atoms on the edge of the molecule (C_3). Low-angle impacts on inner carbon atoms again are less likely to result in adsorption but the sticking probability increases with the projectile energy. In this case, over 20 per cent of collisions on C_3 are reactive when the H atoms carry 1.0 eV. Sticking probabilities show that the PAH efficiently accommodates the reaction and impact energies. The chemical adsorption of H depends more on how the topology of the potential energy surface (PES) around carbon hinders the approach of hydrogen to the surface.

To better understand how the PAH absorbs collision energy and energy from the exothermic adsorption of hydrogen, we analysed the average kinetic energy of the incoming hydrogen and the reaction centre that is impacted, which includes the target carbon and any bonded hydrogen. This sum is referred to as the kinetic energy of the reaction centre, and we plotted its changes over time in Fig. 4. At the start of the collision, this energy is equal to the projectile's kinetic energy, as the PAH has none. The kinetic energy of the reaction centre decreases quickly over time for all impact sites and energies, demonstrating the molecule's ability to absorb excess energy for chemisorption of the hydrogen. After 500 fs, the reaction centres in the molecule's inner regions (C_2 and C_3) have cooled to around 0.2 eV, a third of the energy required to desorb the hydrogen (refer to ΔE° in Table 1). This warranties that once H is chemisorbed on a C atom, it remains bonded. The reaction centre at the molecule's

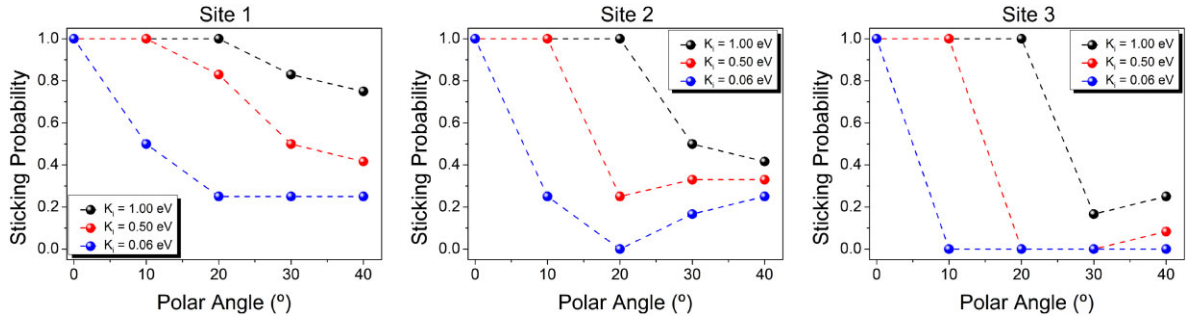

Figure 3. Sticking probability for chemisorption of H on coronene.

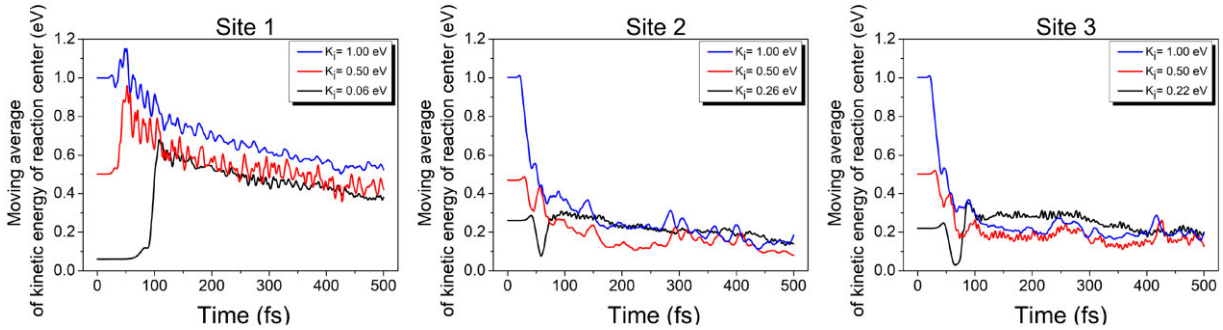

Figure 4. Moving average of kinetic energy of the reactive site for the three non-equivalent sites (C_1, C_2, and C_3) of the coronene.

Downloaded from https://academic.oup.com/mnras/article/524/3/3741/7224009 by guest on 27 March 2024

Table 2. Reaction energy ΔE°, impact energies of hydrogen projectiles K_i, average energy to dissipate E_D, and the ratio between the rotational energy of H_2 and its characteristic energy of rotation $\langle E_r/k_B\Theta_r\rangle$. All energies values in eV. $E_D = \langle \Delta V\rangle + K_i$, where $\langle \Delta V\rangle$ is the average change in potential energy.

Site $C_i(i=1-3)$	ΔE°	K_i	E_D	$\langle E_r/k_B\Theta_r\rangle$
		0.06	2.0	0.54
1	−2.7	0.50	2.4	12.50
		1.00	3.0	17.77
		0.26	2.3	0.15
2	−3.4	0.50	2.5	0.30
		1.00	3.0	0.50
		0.22	2.3	0.11
3	−3.5	0.50	2.6	0.16
		1.00	3.0	0.18

edge (C_1), however, does not cool as much as the inner centres and maintains around 0.5 eV of kinetic energy after 500 fs. The reason for this is that carbon atoms at the edge of the molecule have fewer neighbour carbon atoms to couple vibrationally and dissipate energy with. Overall, there is an interplay between the topology of the PES around a given site and its ability to cool the projectile: at the edge it sticks easier at low polar angle, but is less efficient at accommodating energy.

3.2 H_2 formation via Eley–Rideal mechanism

The next step in the ER mechanism is the abstraction of the chemisorbed hydrogen atom by an incoming H atom, giving rise to the hydrogen molecule and recovering the coronene molecule, coronene-H + H · →coronene + H_2. The abstraction happens through a radical recombination. Both the incoming hydrogen atom and the monohydrogenated coronene are open shell, while the reaction products are closed shell in their ground states. Thus, abstraction can, in principle, proceed through two different reaction channels: singlet and triplet electronic states. However, the singlet mechanism is more likely because it is barrierless (Rauls & Hornekær 2008; Rasmussen, Henkelman & Hammer 2011) and quite exothermic (−2.7 to −3.5 eV, see Table 2) while the triplet has an activation barrier (∼0.4 eV) (Barrales-Martínez et al. 2018). Hence, here we only focus on molecular dynamics on the singlet state. Although it is computationally cheaper to use a closed-shell wave function for the singlet, it results in an incorrect representation of the PES at large distances between hydrogens. Therefore, we will always use a wavefunction with broken spin symmetry that allows us to recover the correct dissociation limit of H_2.

As in the previous case, the projectiles are initially 5 Å away from the target atom (in this case the chemisorbed hydrogen atom) to prevent interactions between the surface and the projectile at the beginning of the molecular dynamics. The same impact energies were used as in the previous step. Our findings indicate that the abstraction of H_2 is a highly probable process. In sites 2 and 3, regardless of the impact parameters, all projectiles achieve the abstraction of the chemisorbed hydrogen atom and the formation of H_2. In site 1, ∼ 92 per cent of the incoming projectiles successfully abstracted the chemisorbed hydrogen atom, while the remaining ∼ 8 per cent resulted in H projectiles with large polar angle ($\theta \geq 30^{\circ}$) that spillover to a neighbour carbon, leading to a doubly hydrogenated molecule. This phenomenon was also observed in previous research (Rauls & Hornekær 2008), which showed that the process is barrierless and aligns with our results.

Since H_2 abstraction is an exothermic reaction, the coronene and the nascent H_2 molecule must accommodate not only the kinetic energy of the incident H atom but also the energy released in the reaction (see Table 2). Despite the coronene having enormous mass compared to H, it accommodates about ∼ 15 per cent of total excess of energy (1–3 eV) as vibrational energy, which corroborates the ability of coronene (PAHs in general) to act as a sink of energy for the H_2 formation in the ISM. In a recent computational study, Pantaleone et al. (2021) found that water-ice surfaces absorb ∼ 50 per cent of the energy released in the H_2 formation. In their simulation, H atoms carried no initial kinetic energy, which gave time for a longer interaction between H and surface and a more effective dissipation of energy.

The remaining ∼ 85 per cent of the excess of energy is carried by the nascent hydrogen molecule. After its release, the H_2 molecule acquires a large translational kinetic energy, which on average represents between 20 and 60 per cent (∼0.4–1.25 eV) of the excess of energy, E_D. The translational energy of H_2 molecules depends weakly on the polar angle of the orientation of incoming H · projectile, as it can be seen in Fig. 5. Although two slight trends are observed. H_2 molecules released from the edge carbon (C_1) exhibit an increase of the translational energy as the incoming projectile deviates from normal impact. Contrary, molecules released from inner carbons (C_3 and C_3) carry less translational energy as the impact deviates from normal.

3.3 Rotational and vibrational states of the nascent H_2

The vibrational state (υ) of the released H_2 was approximated by matching the vibrational energy (measured ∼30 fs after H_2 bond breaking with coronene) to closest eigenvalue of a Morse potential that fits H_2 dissociation PES (see Section 3 in Supporting

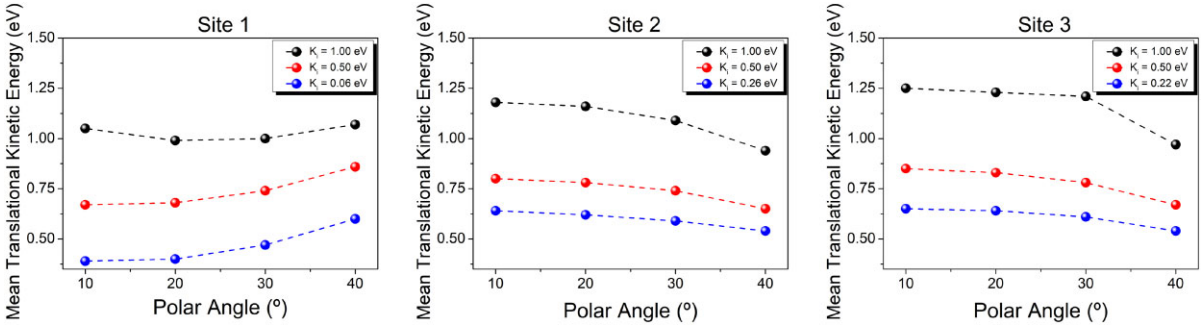

Figure 5. Mean translational kinetic energy of the H_2 molecules averaged over the azimuthal angle of the incoming H projectile for each site: C_1, C_2, and C_3.

Downloaded from https://academic.oup.com/mnras/article/524/3/3741/7224009 by guest on 27 March 2024

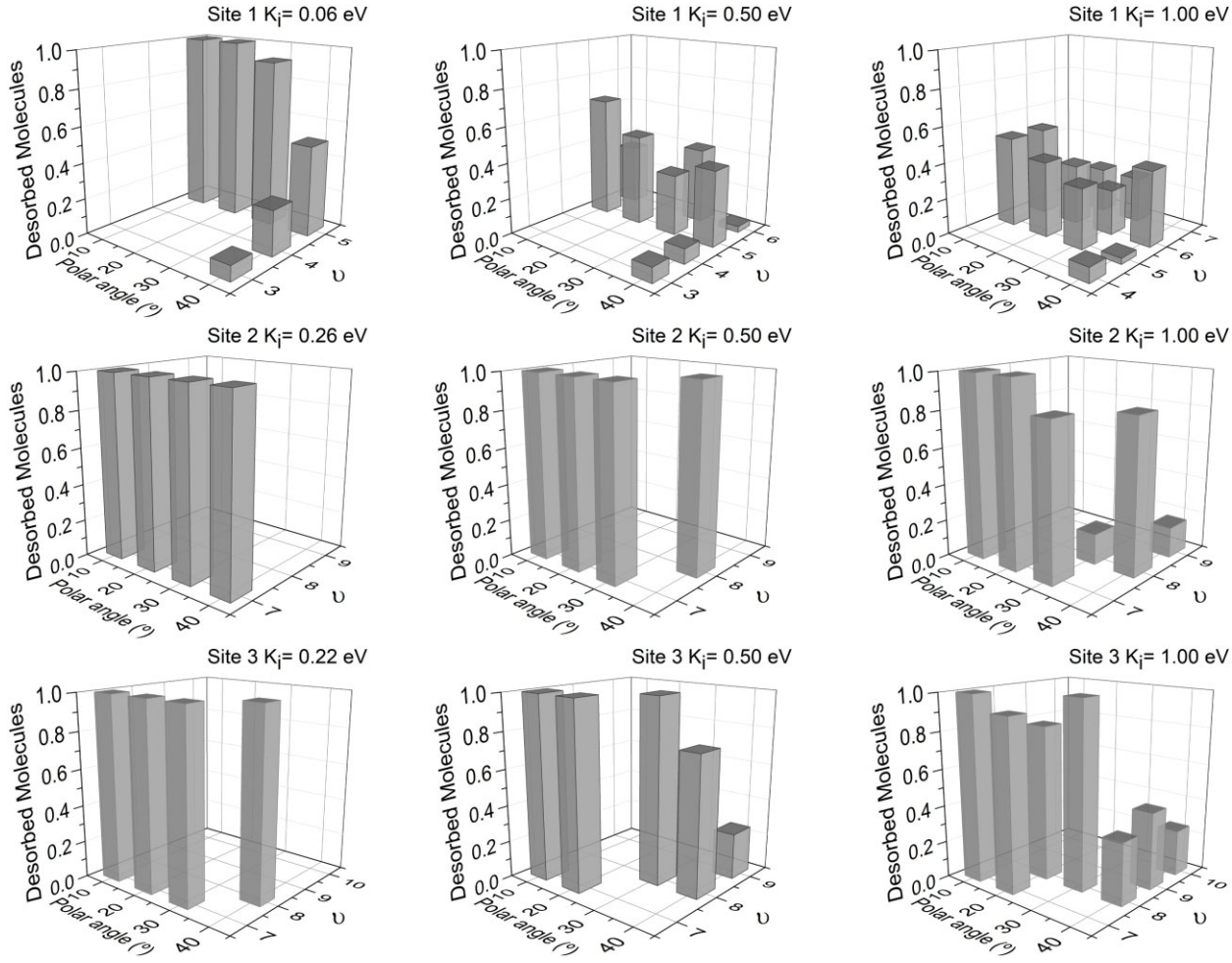

Figure 6. Vibrational population for the H_2 nascent on to the three sites.

Information). Fig. 6 shows the fraction of molecules formed with a given υ that come from impacts at different polar angles. All H_2 molecules desorb in vibrational excited states with υ as low as 3 and as large as 10. These degree of vibrational excitations align with other evidence. For instance, H_2 formed on graphite surfaces occupies vibrational levels around $\upsilon = 3$–5 (Latimer et al. 2008; Casolo, Tantardini & Martinazzo 2013) and that formed on water surfaces occupies higher levels ($\upsilon = 1$–8) (Roser et al. 2003; Yabushita et al. 2008). Vibrational excitation depends on the impact energy and orientation of H · projectiles. When H · impacts on the H chemisorbed on the outermost carbon (C_1) at low angles (40°), the released H_2 occupies lower vibrational states ($\upsilon \geq 3$) with a broader distribution of υ ($3 \leq \upsilon \leq 7$). However, for inner sites, the vibrational populations of the newly formed H_2 molecules behave differently. When the projectile moves away from normal collision, the molecules tend to have a higher vibrational state (ranging in $7 \leq \upsilon \leq 10$). As the impact energy increases, the occupation of vibrational states broadens. However, for the external site, there is a significant dependence on the impact angle. Molecules desorbing from the external carbon carry less vibrational energy than those detached from internal carbons. This marked difference in vibrational energy is traced to the different topologies of the PES around these sites.

The rotational energy (E_r) of the released H_2 was calculated from the angular momentum at the turning points. Rotation is the degree of freedom that accommodates the smallest part of the excess energy, not exceeding 10 per cent in all cases. This is a reasonable situation because the H_2 molecule has a low moment of inertia, and hence a large rotational constant/temperature ($\Theta_r = 85.3$ K; McQuarrie 2000). Our simulations show that in the low impact-energy regime, released molecules are far from achieving the thermodynamic limit of the distribution of rotational states ($E_r/k_B\Theta_r < 1$), see Fig. 7. The dependence of rotational energy on impact energy is strongly dependent on where the abstraction takes place. Even at collision energies as high as 1 eV, the molecules released from the inner carbons do not reach the thermodynamic limit of the rotational energy distribution, ($E_r/k_B\Theta_r < 1$). Instead, in the edge carbon all the molecules are released with $E_r > > k_B\Theta_r$. Note that even in the latter case, the rotational cooling capacity of the reaction site is limited and saturates with increasing impact energy (compare C_1 $K_i = 0.5$ eV and $K_i = 1.0$ eV). Yabushita et al. (2008) found that H_2 products (in thermal equilibrium) of the photolysis of amorphous water-ice H carry rotational energies in the range of $1 - 15 \times 10^{-20}$ J, which is equivalent to $E_r/k_B\Theta_r < 15$. This aligns with our result that rotational energy of H_2 saturates at about $E_r/k_B\Theta_r = 15$–20 (see upper right panel in Fig. 7).

Downloaded from https://academic.oup.com/mnras/article/524/3/3741/7224009 by guest on 27 March 2024

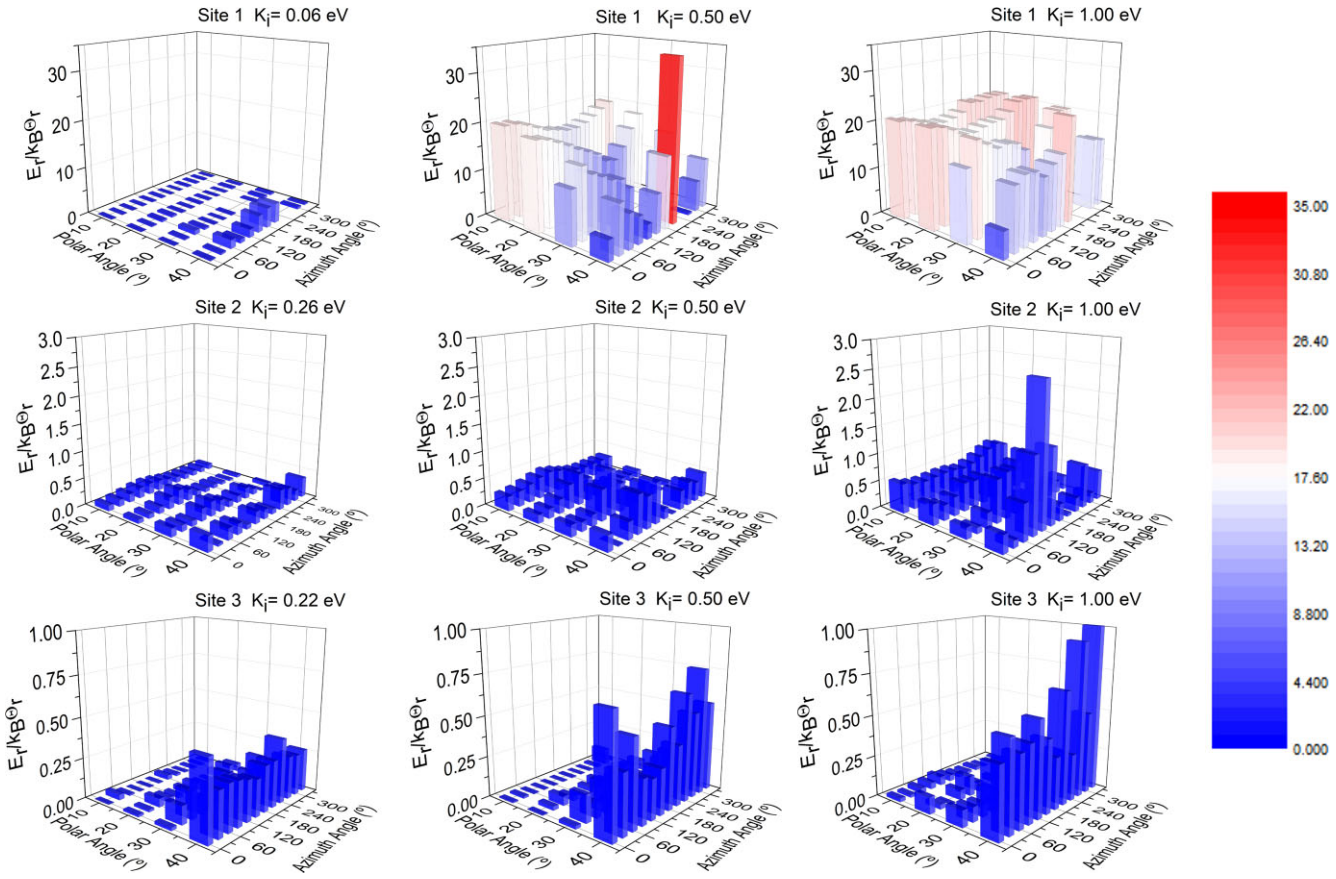

Figure 7. Ratio between the rotational energy of the newly formed H_2 molecule and its characteristic energy of rotation ($k_B\,\Theta_r$).

3.4 Implications of vibrationally excited H_2 in the ISM

Vibrationally excited H_2 in space is primarily generated through different mechanisms and sources. Shock waves and far-ultraviolet fluorescence are two main sources, as indicated by Beckwith et al. (1978), Gatley et al. (1987), Sternberg (1989), Sheffer et al. (2009), Gnaciński (2013), and Rachford, Snow & Ross (2014). Additionally, X-ray photons and cosmic rays (Gaches et al. 2022; Padovani et al. 2022) have been suggested as potential sources, along with H_2 formation itself (Wakelam et al. 2017). For example, Chang et al. (2021) observed that over 90 per cent of the H_2 formed from the UV photodissociation of H_2O exhibited vibrational excitation at $\upsilon = 3$. Similarly, Zhao et al. (2022) conducted a study on the fragmentation dynamics of $H_2S + h\nu \longrightarrow S(^1S) + H_2(X^1\Sigma_g^1)$ and found that H_2 molecules formed with a wide range of vibrational states, with a peak at $\upsilon = 5$. Regarding reactions on surfaces, Gough et al. (1996) discovered that H_2 formed on graphite and other carbonaceous surfaces can populate high vibrational states, such as $\upsilon = 7$.

Based on our simulations, we have observed that nascent hydrogen molecules desorbing from the edge sites of coronene, and likely from all PAHs, exhibit excited vibrational states similar to those found in the experiments conducted by Gough et al. (1996) and Chang et al. (2021). Interestingly, hydrogen molecules formed in internal sites of PAHs show even higher levels of vibrational excitation compared to those generated through photochemical reactions. On the other hand, the lifetime of vibrationally excited hydrogen molecules is of the order of days (Draine 2000; Sheffer et al. 2009; Chang et al. 2021), mainly due to their Einstein A-coefficients, which range from approximately 10^{-7} to $10^{-6}s^{-1}$ (Wolniewicz, Simbotin & Dalgarno 1998; Coppola et al. 2016). This implies that H_2 molecules formed on PAHs through the ER mechanism could serve as active reagents in the ISM chemistry. Vibrationally excited H_2 molecules can participate in chemical reactions that are otherwise challenging to occur in the ground state, as their internal vibrational energy enables them to overcome activation barriers (Agúndez et al. 2010). This is particularly relevant for the initial stages of heavy element chemistry, involving the formation of hydrides through gas-phase reactions

$$X + H_2 \longrightarrow XH + H, \tag{1}$$

where X could be carbon, oxygen, nitrogen, and sulfur atoms or their cations (Stecher & Williams 1972; Zanchet et al. 2019; Goicoechea & Roncero 2022).

4 CONCLUSIONS

We studied the energy dissipation in the H_2 formation process via the ER mechanism on to a coronene surface by means of Born–Oppenheimer (*ab initio*) molecular dynamics. Our simulations show that for the chemisorption of hydrogen (first step of the ER mechanism), the sticking probability depends on both the kinetic energy of the projectile and in its orientation (polar angle). The general tendency observed is that the sticking probability decreases as the projectile moves away from the normal orientation. Moreover, internal sites (C_2 and C_3, see Fig. 1) exhibit a lower sticking probability compared with the edge site (C_1). In contrast, it is the internal sites that are capable of dissipating a greater amount of the

Downloaded from https://academic.oup.com/mnras/article/524/3/3741/7224009 by guest on 27 March 2024

excess energy acquired due to chemisorption in a shorter time-scale compared to the edge site.

For the second step of the ER mechanism, the abstraction and formation of H_2, our simulations show that the reaction is a highly probable process under the studied conditions. All incoming projectiles achieve abstraction at the inner sites and over 90 per cent at the edge site. About ~ 15 per cent of the energy is dissipated to the coronene molecule as vibrational energy. The remaining energy is transferred to the nascent hydrogen molecule. H_2 detaches from coronene with a large amount of translational kinetic energy (≥ 0.4 eV) and in a highly excited vibrational state ($\upsilon \geq 3$). The activation of the rotational degrees of freedom is the mechanism that least contributes to the partition of the excess energy linked to the reaction (≤ 10 per cent).

We also discussed how the formation of molecular hydrogen on PAHs through ER mechanism may represent a further source of vibrationally excited H_2 observed in the ISM and play the role of activated reagent on the ISM chemistry.

ACKNOWLEDGEMENTS

This research was funded by FONDECYT through projects 1220366, 1231487, and 1220715 and by the Center for the Development of Nanosciences and Nanotechnology, CEDENNA AFB 220001. NFB gratefully acknowledges ANID for National MSc Fellowship in the year 2022 (number 22220676). Powered@NLHPC: This research was partially supported by the supercomputing infrastructure of the NLHPC (ECM-02).

DATA AVAILABILITY

All data necessary to reproduce and check this work (molecular structures and MD trajectories) are available in the GitHub repository at https://github.com/nfbarrera/Formation-of-H2-on-polycyclic-aromatic-hydrocarbons.

REFERENCES

Agúndez M., Goicoechea J. R., Cernicharo J., Faure A., Roueff E., 2010, ApJ, 713, 662
Barrales-Martínez C., Gutiérrez-Oliva S., 2019, MNRAS, 490, 172
Barrales-Martínez C., Cortés-Arriagada D., Gutiérrez-Oliva S., 2018, MNRAS, 481, 3052
Bauschlicher C. W. J., 1998, ApJ, 509, L125
Beckwith S., Persson S. E., Neugebauer G., Becklin E. E., 1978, ApJ, 223, 464
Boschman L., Cazaux S., Spaans M., Hoekstra R., Schlathölter T., 2015, A&A, 579, A72
Burke D. J., Brown W. A., 2010, Phys. Chem. Chem. Phys., 12, 5947
Casolo S., Tantardini G. F., Martinazzo R., 2013, Proc. Natl. Acad. Sci., 110, 6674
Cazaux S., Spaans M., 2009, A&A, 496, 365
Cernicharo J., Agúndez M., Cabezas C., Tercero B., Marcelino N., Pardo J. R., de Vicente P., 2021, A&A, 649, L15
Chang Y. et al., 2021, Nat. Commun., 12, 6303
Chen T., Xiao C. Y., Li A., Zhou C. T., 2021, MNRAS, 509, 5231
Coppola C. M., Mizzi G., Bruno D., Esposito F., Galli D., Palla F., Longo S., 2016, MNRAS, 457, 3732
Cortés-Arriagada D., Gutiérrez-Oliva S., Herrera B., Soto K., Toro-Labbé A., 2014, J. Chem. Phys., 141, 134701
Draine B. T., 2000, ApJ, 532, 273
Elstner M., Seifert G., 2014, Phil. Trans. R. Soc. A, 372, 20120483
Elstner M., Porezag D., Jungnickel G., Elsner J., Haugk M., Frauenheim T., Suhai S., Seifert G., 1998, Phys. Rev. B, 58, 7260
Foley N., Cazaux S., Egorov D., Boschman L. M. P. V., Hoekstra R., Schlathölter T., 2018, MNRAS, 479, 649
Foulkes W. M. C., Haydock R., 1989, Phys. Rev. B, 39, 12520
Frisch M. et al., 2009, Gaussian 09, revision D. 01. Gaussian, Inc., Wallingford CT, USA
Gaches B. A. L., Bialy S., Bisbas T. G., Padovani M., Seifried D., Walch S., 2022, A&A, 664, A150
Gatley I. et al., 1987, ApJ, 318, L73
Gnaciński P., 2013, A&A, 549, A37
Goicoechea J. R., Roncero O., 2022, A&A, 664, A190
Gough S., Schermann C., Pichou F., Landau M., Cadez I., Hall R., 1996, A&A, 305, 687
Gould R. J., Salpeter E. E., 1963, ApJ, 138, 393
Hourahine B. et al., 2020, J. Chem. Phys., 152, 124101
Inostroza N., Mardones D., Cernicharo J., Zinnecker H., Ge J., Aria N., Fuentealba P., Cardenas C., 2019, A&A, 629, A28
Inostroza-Pino N., Mardones D., Ge J. J. X., MacLeod-Carey D., 2020, A&A, 641, A14
Inostroza-Pino N., MacLeod-Carey D., Heyser C., Mardones D., Espinoza C., Ge J., 2021, A&A, 650, A169
Köhler C., Seifert G., Frauenheim T., 2005, Chem. Phys., 309, 23
Koskinen P., Mäkinen V., 2009, Comput. Mater. Sci., 47, 237
Latimer E. R., Islam F., Price S. D., 2008, Chem. Phys. Lett., 455, 174
Le Page V., Snow T. P., Bierbaum V. M., 2009, ApJ, 704, 274
Lemaire J. L., Vidali G., Baouche S., Chehrouri M., Chaabouni H., Mokrane H., 2010, ApJ, 725, L156
McCarthy M. C., McGuire B. A., 2021, J. Phys. Chem. A, 125, 3231
McGuire B. A. et al., 2021, Science, 371, 1265
McQuarrie D. A., 2000, Statistical Mechanics. University Science Books, Sausalito, CA, USA
Mennella V., Hornekær L., Thrower J., Accolla M., 2012, ApJ, 745, L2
Padovani M. et al., 2022, A&A, 658, A189
Pantaleone S., Enrique-Romero J., Ceccarelli C., Ferrero S., Balucani N., Rimola A., Ugliengo P., 2021, ApJ, 917, 49
Perdew J. P., Burke K., Ernzerhof M., 1996, Phys. Rev. Lett., 77, 3865
Pirronello V., Liu C., Shen L., Vidali G., 1997, ApJ, 475, L69
Rachford B. L., Snow T. P., Ross T. L., 2014, ApJ, 786, 159
Rasmussen J. A., Henkelman G., Hammer B., 2011, J. Chem. Phys., 134, 164703
Rauls E., Hornekær L., 2008, ApJ, 679, 531
Roser J. E., Swords S., Vidali G., Manicó G., Pirronello V., 2003, ApJ, 596, L55
Sheffer Y., Prochaska J. X., Draine B. T., Perley D. A., Bloom J. S., 2009, ApJ, 701, L63
Stecher T. P., Williams D. A., 1972, ApJ, 177, L141
Sternberg A., 1989, in Kaldeich B. H., ed, Infrared Spectroscopy in Astronomy. European Space Agency (ESA), Paris, France
Thrower J. et al., 2012, ApJ, 752, 3
Tielens A. G. G. M., 2008, ARA&A, 46, 289
van de Hulst H. C., 1948, Harv. Obs. Monogr., 7, 73
Vidali G., 2013, Chem. Rev., 113, 8752
Wakelam V. et al., 2017, Mol. Astrophys., 9, 1
Weingartner J. C., Draine B. T., 2001, ApJS, 134, 263
Wolniewicz L., Simbotin I., Dalgarno A., 1998, ApJS, 115, 293
Yabushita A., Hama T., Iida D., Kawanaka N., Kawasaki M., Watanabe N., Ashfold M. N. R., Loock H.-P., 2008, ApJ, 682, L69
Zanchet A., Lique F., Roncero O., Goicoechea J. R., Bulut N., 2019, A&A, 626, A103
Zhao Y. et al., 2022, J. Phys. Chem. Lett., 13, 9786

SUPPORTING INFORMATION

Supplementary data are available at *MNRAS* online.

Optimized Cartesian Coordinates and Energies.
Table S1. Quantification of the conservation of energy for a set of AIMDs with DFTB and DFT.

Downloaded from https://academic.oup.com/mnras/article/524/3/3741/7224009 by guest on 27 March 2024

Figure S1. Moving average of the change in potential energy for the dynamics calculated at the PBE/6-31G(d) and DFTB/MIO theoretical levels at site C_1.
Figure S2. Moving average of the change in potential energy for the dynamics calculated at the PBE/6-31G(d) and DFTB/MIO theoretical levels at site C_2.
Figure S3. Moving average of the change in potential energy for the dynamics calculated at the PBE/6-31G(d) and DFTB/MIO theoretical levels at site C_3.

Figure S4. Morse potential and its eigenvalues for H_2.

Please note: Oxford University Press is not responsible for the content or functionality of any supporting materials supplied by the authors. Any queries (other than missing material) should be directed to the corresponding author for the article.

This paper has been typeset from a TEX/LATEX file prepared by the author.

Downloaded from https://academic.oup.com/mnras/article/524/3/3741/7224009 by guest on 27 March 2024

© 2023 The Author(s)
Published by Oxford University Press on behalf of Royal Astronomical Society